HALF-SCALE TRANSONIC COMPRESSOR RAPID TESTING RIG

Tianhou Wang
Whittle Laboratory
University of Cambridge

James Taylor
Whittle Laboratory
University of Cambridge

ABSTRACT

High-speed compressor testing is costly due to mechanical complexity and hazardous due to the high energy involved. In the past this has limited the speed and amount of testing. In this paper a new rig architecture is presented that aims to test a scaled transonic compressor stage rapidly. It builds upon the low-speed rapid testing developments made at the Whittle Laboratory and has potential to accelerate technology development.

The power input requirement is reduced by testing at half-scale and reduced Reynolds number while maintaining the Mach number. Further power saving and mechanical simplification is achieved by employing a turbo-expander architecture with no shaft-power input, only the aerodynamic losses in system must be overcome.

The aerodynamic and mechanical design of the rig is presented. Safe operation and rapid access and rebuild times are critical. The test hardware is machined from solid and bladed disks and rings can be manufactured in days. Only standard instrumentation is required, although a novel control loop is employed to achieve the same accuracy in rotational speed as an electric motor driven compressor rig.

Experiments up to 25% design rotational speed were conducted, and the results presented here show that the rig is controllable and inherently safe if the research compressor fails. The rig will be run to full speed in the immediate future and extension to the capability is planned with multi-stage high-speed testing in a second machine.

INTRODUCTION

In compressor research and design, high-speed testing is usually used for demonstration purposes at high TRL. Because of the realism of the experiment the monetary and time expense is routinely measured in millions and years. The megawatts of power involved requires large, dedicated facilities to be constructed, making such experiments financially inaccessible to all but a few laboratories [1]. Delays and losses due to failure of complex mechanical systems are encountered in almost every campaign.

To mitigate these drawbacks, for aerodynamic experiments, scaling is applied to match the non-dimensionals while allowing rig simplifications. The common compromise is to match the Reynolds number but not the Mach number, resulting in large low-speed rigs 6 ft in diameter, examples include the General Electric 4-stage 'LSRC' [2], the Whittle Laboratory Freeman rig [3] and Deverson rig [4]. This is useful for testing stages not affected by compressibility effects but misses the key physics of choking and shock waves of transonic stages. The change in density and the resultant stage matching implications are also missed. While the increased size can improve measurement resolution it inevitably increases manufacture timescales and creates handling difficulties.

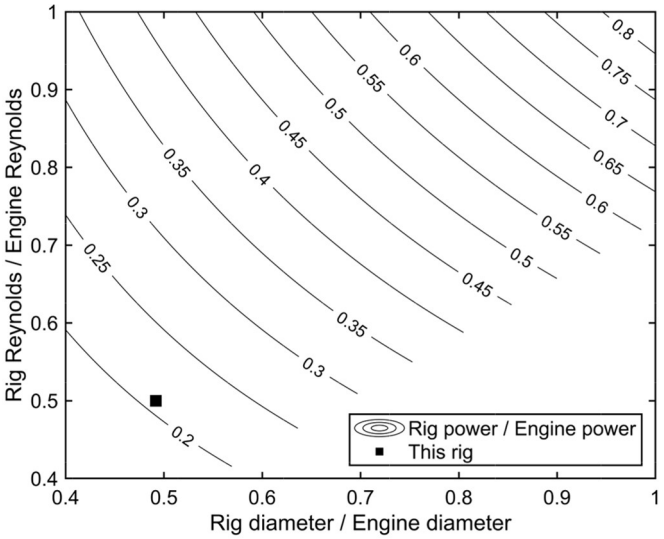

Figure 1: High-speed low power compressor testing

Recently some low-speed machines have been developed to achieve rapid testing with changeover times measured in minutes. An example at the Whittle Laboratory on the Gibbons compressor tested 125 different builds of damaged compressor blades [5]. The aim of this paper is to develop this capability into a high-speed rapid testing rig. We take the alternative to the scaling compromise, the Mach number is matched, diameter is reduced along with the Reynolds number. This allows power savings of 80% as shown in Figure 1.

The high TRL mindset is also deliberately resisted, in this case there is no need to match everything and demonstrate mechanical design as well as aerodynamic. Instead, all aspects of the aerodynamic testing are to be kept as simple as possible, focusing on what can be done to increase the speed of testing.

In the following sections, the test case, rig architecture, and the power savings are first presented. Aerodynamic and mechanical designs of this unconventional rig are discussed in detail along with the manufacturing methods. Current and planned instrumentation are discussed, as well as the methods to control and operate the rig. Preliminary low-speed results are

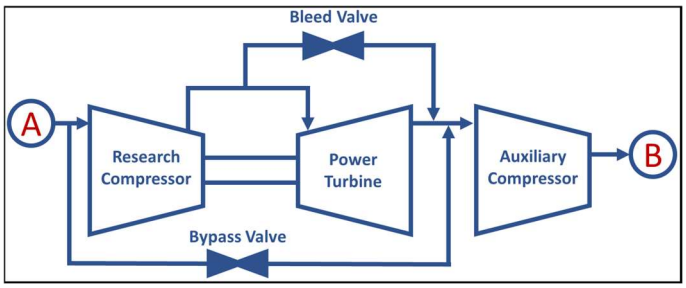

Figure 2: Block diagram of the rig, open-loop: A and B to atmosphere, closed-loop: A and B connected through a water-cooled intercooler

finally shown which shows that the rig is safe, controllable, and can achieve high quality data. The next steps of the experimental campaign are discussed before the conclusions.

TEST CASE

The shaft power required by a compressor of fixed design is proportional to the Reynolds number, Mach number squared, inlet temperature and the diameter of the machine:

$$\dot{W}_x \propto Re \times M^2 \times T \times D$$

The research compressor presented in this paper is a transonic compressor stage from a modern aero engine. It is critical to match the Mach number from the engine in the rig test but power savings can be made with deliberate reduction of the remaining parameters. Temperature is reduced as the rig runs with an atmospheric inlet rather than being embedded within a high pressure ratio aero engine. Reynolds number is also reduced when running open-loop with an atmospheric inlet but could be recovered with closed-loop operation with pressurisation and intercooling. Power savings from size reduction are always possible. The relationship between power saving, size, and Reynolds number is plotted in Figure 1 for this test case.

A summary of the power savings components of this approach for the research compressor presented in this paper are given in the table:

	Engine	Rig
Reynolds number	1.4×10^6	0.7×10^6
Blade Mach number	1.2	1.2
Inlet temperature / K	340	290
Diameter / mm	610	300
Power / MW	1.3	0.27

The test compressor achieves a power saving of 80% relative to the engine at an acceptable Reynolds number. However, it requires double the shaft rotational speed. This could increase the complexity and expense with step-up gear boxes, a high-speed motor, or gas turbine. Instead, in this paper a mechanically simpler approach is taken: The research compressor is connected to a power turbine mounted on the same shaft. All that is required to drive the machine up to speed is an auxiliary compressor to provide a source of vacuum. The rig is a simple turbo-expander with only one air stream. A block diagram of the rig is shown in Figure 2.

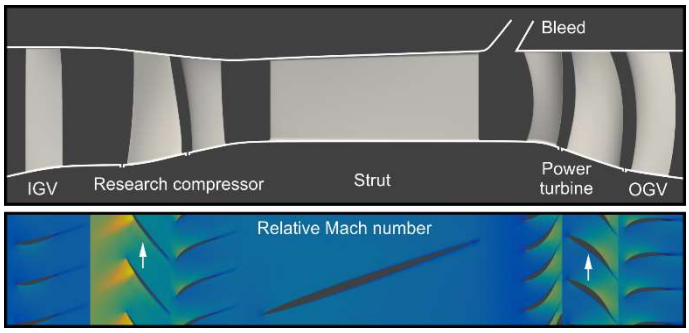

Figure 3: Meridional view of rig and blading at 70% span

AERODYNAMIC DESIGN

In this section of the paper the aerodynamic design of the turbo-expander is covered. The arrangement requires seven blade rows to be created along with a single bleed. The rig is designed using the 3D RANS solver TURBOSTREAM [6]. Cell counts of 1M per passage are used with the Spalart-Allmaras turbulence model [7] and a Y+ of 1. The resulting geometry is shown along with a slice through the flow solution in Figure 3:

- Inlet guide vanes (IGVs) are used to turn the flow to match the stage's incoming swirl distribution in the engine.
- The research compressor is scaled from a modern transonic aero-engine compressor stage, the gapping, thickness, and clearances are all maintained.
- A low-aspect ratio structural strut is aligned with the stator exit whirl angle; no turning is performed in this row.
- The stator and rotor of the power turbine are automatically designed in CFD to provide power to the research compressor stage.
- Outlet guide vanes (OGVs) are used to recover the exit swirl before passing flow into the diffuser.
- Variable bleed is taken upstream of the power turbine, this allows the working line of the machine to be moved and the operating characteristic of the research compressor to be mapped out.

To validate the design of the whole turbo-expander system a compressor characteristic is mapped out using 3D CFD and is plotted alongside the performance maps of the research compressor itself, the power turbine, and the auxiliary compressor in Figure 4. The cases with bleed control include a fully meshed bleed slot to remove a specified fraction of mass flow rate from the main passage.

The first plot shows the design point of the compressor at 100% speed. The turbine has been created to provide the required power to match the design point when 24% of flow is being bled off through the slot. This is essential as it allows the bleed to be closed to increase power output from the turbine and throttle the compressor up its characteristic. The last stable operating point of the compressor occurs with 10% bleed. If the bleed is closed further the compressor drops into rotating stall, the last point run in this CFD simulation is with 5% bleed. This extra margin of bleed will allow the research compressor to be stalled in the experiment even if the CFD is currently underpredicting the operating range, or if the bleed valve has some leakage due to mechanical reasons, or to allow testing

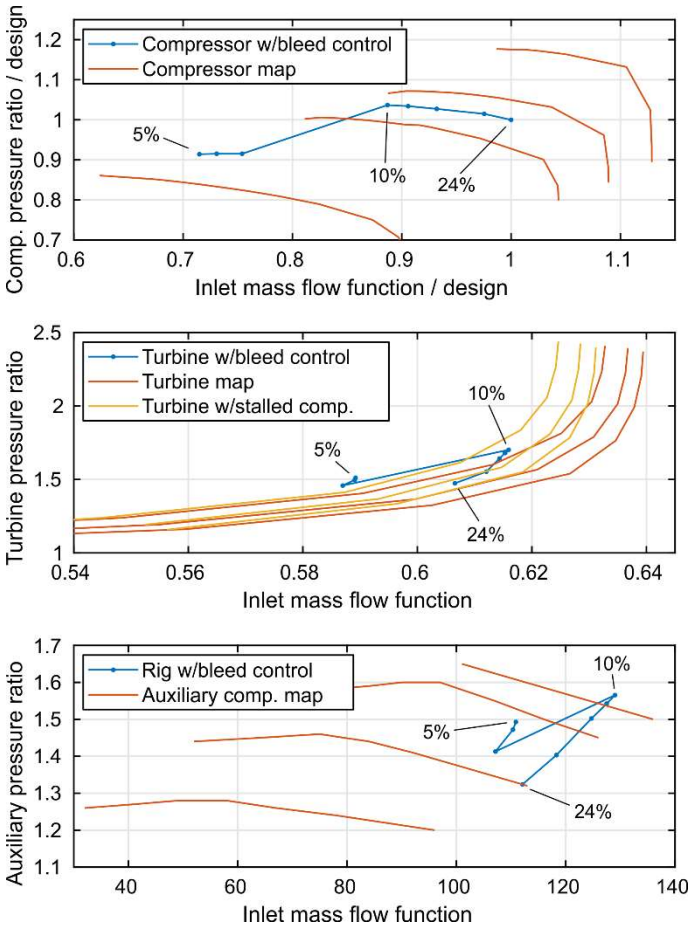

Figure 4: Operating characteristics of the research compressor, power turbine and auxiliary compressor

other geometries with larger operating range in the future without replacing the turbine.

The second plot shows the operating points of the turbine as the compressor is throttled into stall. It is overlaid on two turbine maps. One map run with a boundary condition from when the compressor is operating on the stable part of the characteristic. And the other map run with a boundary condition taken from the exit of the stalled compressor, this has a tip-low profile. As bleed is varied the turbine pressure ratio increases and crosses multiple non-dimensional speed lines. As the compressor stalls the inlet flow into the turbine drops as does the pressure ratio.

The final plot shows the operating point of the downstream auxiliary compressor. This is a centrifugal machine that forms part of the variable density high-speed wind tunnel at the Whittle Laboratory. As the bleed rate of the turbo-expander rig is reduced to map out the constant speed characteristic of the research compressor the pressure ratio of the downstream compressor increases from 1.32 up to 1.56 before dropping back down again. In practice this machine will be run at its maximum speed and flow will be bypassed around the whole turbo-expander rig by components not shown in Figure 2, this will allow more rapid control. On top of this, a fine bypass valve is installed on the rig itself, shown in Figure 2.

It is worth noting that the rig is self-starting, and no pre-spinning is necessary for air flow to be established. This means

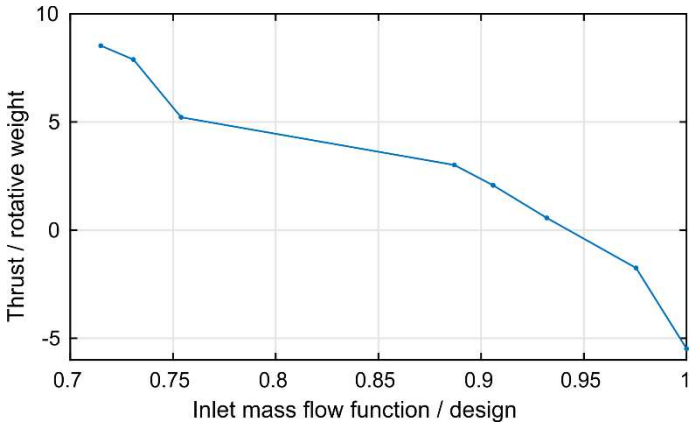

Figure 5: Thrust direction change over operating range

the rig can also recover from research compressor stall by means of its own controls.

MECHANICAL DESIGN AND MANUFACTURING

High-speed compressor testing usually requires a large quantity of mechanical design work and manufacturing expense. The simple design presented in this paper aims to reduce this along with the requirements for costly bought in items. This machine only requires the bearing set, standard fasteners, and simple electronics.

Three aspects of the mechanical design and manufacturing are covered in this section: First, the design of the bearing assembly and rotatives. Second, design of the fast change over system for the research compressor. Third, the manufacturing processes used to create the hardware in-house.

The bearing arrangement for this turbo-expander needs to take thrust loads in both directions. Figure 5 shows the calculated thrust on the rotating assembly over the flow range of the compressor characteristic modelled in CFD. On the right, at the design point, the thrust is upstream with a value of 5 times the weight of the rotating assembly. As the compressor is throttled into stall the direction of the thrust changes and acts downstream with increased magnitude.

The bearing arrangement must also be simple, and yet deal with the high rotational design speed of 22,500 RPM. A back-to-back arrangement commonly used in automotive turbochargers is chosen. A section through the bearing assembly at the research compressor end of the rig is shown in Figure 6. The bearing carriage slides axially and holds a 30° angular contact bearing. When the thrust load on the rotating assembly is in the downstream direction this carriage bottoms out. When the thrust reverses, a wave spring is used to maintain the pre-load on the bearing as the carriage on the other side bottoms out instead. This arrangement is also unaffected by thermal expansion; the wave springs allow for substantial changes in length.

The bearings are designed to operate rigidly over the whole rotational speed range. The critical shaft speed is predicted to occur at 30,000 RPM. This requires a combination of high stiffness and lightweight rotating components:

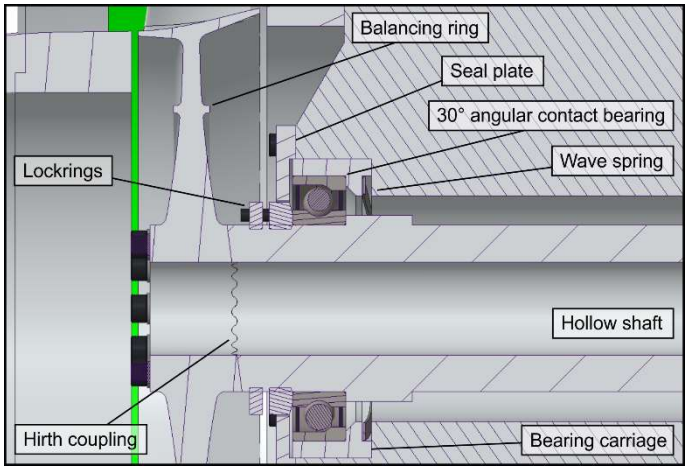

Figure 6: CAD illustration of sub-critical bearing design

- The largest diameter grease packed high-precision steel rolling element bearing is chosen that can withstand the rotational speed.
- The bearing housing and structural struts are machined from a single piece of aluminium.
- The steel base frame is welded from box-section with solid webs throughout the structure, see Figure 10.
- A hollow aluminium shaft, lightweight aluminium blisks and custom lightweight two-piece axially clamping lockrings result in an assembly less than 3 Kg.

The research compressor and power turbine have been designed to be replaced rapidly. Using the overhung disk arrangement allows each end of the rig to be worked on independently. The coupling between the rotor disks and the shaft is a Hirth type as shown in Figure 7. The bolts pass through the faces of the coupling itself, this allows rigid clamping between the shaft and disc, accurate and repeatable positioning, and fast disassembly.

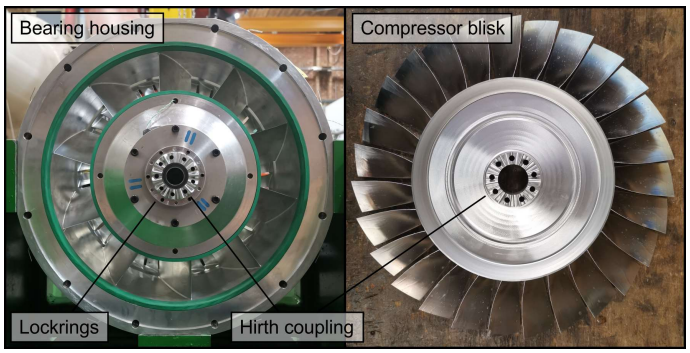

Figure 7: Photograph of shaft and disc couplings

Each row of blades is machined from solid in a single piece: blisks in the case of the two rotating rows, blings in the case of the 5 stationary rows. As well as providing rigidity this reduces the component count and reduces build times. Balancing rings are included on both blisks and the compressor and turbine are balanced in situ on the rig. The rigid mounted bearings and solid blisk design allow balancing to less than G0.4. This high degree of balancing coupled with the stiffness of the disk and blades ensures good clearance control so that the non-dimensional clearances can be matched to the engine.

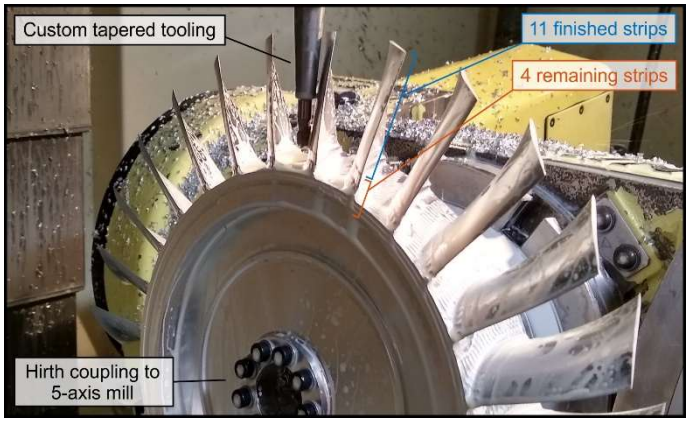

Figure 8: CNC machining the turbine rotor blisk

All rows of the machine are five-axis milled from aluminium alloy, 6082-T6 for stationary components and 7075-T6 for rotating. An in-house code is used to create the toolpaths directly from the blade geometry surfaces. In the case of the blisks the procedure machines the blade from the tip down in 15 strips. Alternating between roughing and finishing ensures that there is always enough rigidity to machine the blade surface with minimal deflection and no chatter. Figure 8 shows the turbine blisk with four remaining strips to be finished. The tapered tool extender maximises rigidity within access constraints. The Hirth coupling is used to mount the blank onto the trunnion table of the mill, this alignment allows the blade tips to be cut to length external to the rig and is a considerable time saving.

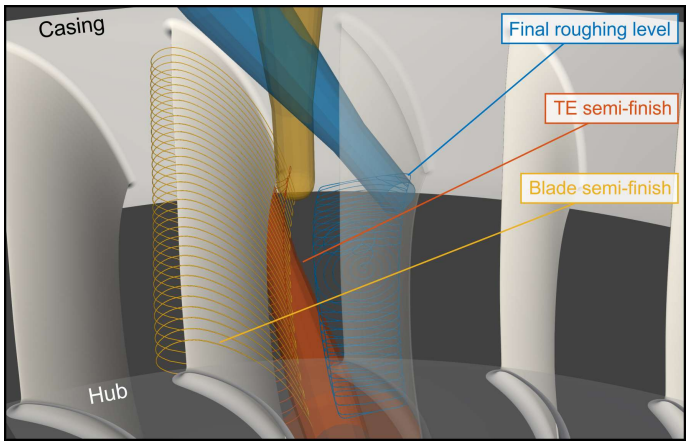

Figure 9: Programming the compressor stator bling

The stationary blings are machined from two sides in three operations as shown in Figure 9. The passages are roughed from the leading edge side, then the part is flipped and the trailing edge circle is finished, finally the part is flipped back and the entire blade is finished from the leading edge side with a simultaneous 5-axis milling operation. This approach ensures that there are no unintended discontinuities anywhere in the blade surfaces. It takes between 24 and 36 hours to machine any of the blade rows in the turbo-expander in this way.

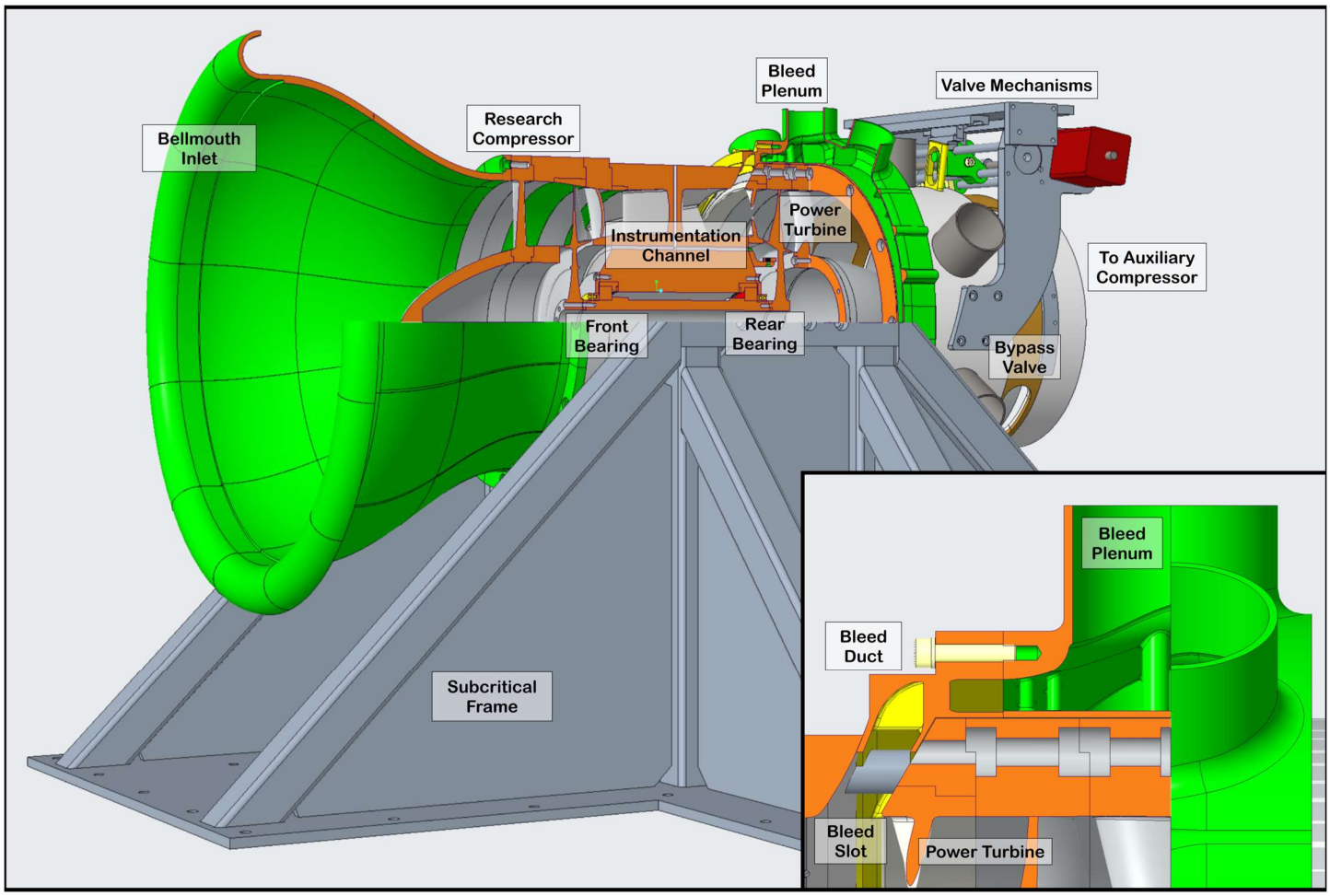

Figure 10: 1/4 cutaway CAD illustration of the rig

INSTRUMENTATION

This section discusses two aspects of instrumentation: First, the currently installed housekeeping instrumentation to control the rig and make preliminary measurements. Second, the research instrumentation that is planned to take detailed measurements of the flowfield.

For mechanical health monitoring purposes, thermocouples are placed in the bearing carriage which raises an alarm if the bearings are overheating. An array of three unsteady pressure probes is installed on the casing at the research compressor rotor leading edge, they perform tip timing and guard against excessive blade vibration. The power turbine rotor blades are twice as thick as the research compressor rotor and are considered not critical in vibration. Shaft speed is measured by a once-per-rev optical pickup mounted on the power turbine side. An accelerometer is installed on the bearing housing and logged synchronously with the once-per-rev sensor to allow the rotor to be balanced and to monitor the crossing of natural modes of vibration.

Static tappings are made on the casing between the blade rows to allow monitoring and pressure rise characteristic measurements. A pitot-static pair is also placed between the IGV and research compressor.

Mass flow rate through the research compressor is measured by a bellmouth previously calibrated against a venturi. The calibration setup is shown in Figure 11. The whole tunnel is raised above the floor such that the floor clearance – bellmouth diameter ratio is representative of the running setup. The bellmouth is instrumented with a Kiel head total pressure probe and wall static tappings, which allows the calculation of a discharge coefficient. The centre body is reproduced in an adapter and supported in the middle with thin aerodynamic struts: this is shown as a multi-coloured part in Figure 11.

Traverse probes are key to good flowfield measurements. Historically, for high quality aerodynamic measurements, large rigs were built, such that probes can be relatively small to reduce blockage and resolve flow features such as trailing edge wakes. Many disbelieve the potential capability of a small rig for this reason. However, the advance of manufacturing methods means that miniature probes can be made to maintain the probe diameter to rig diameter ratio. While a traverse is not installed in the rig yet, there is no fundamental physical limitation preventing small probes to be used in small rigs.

Assuming a rigid clamping on the casing, the end deflection δ of a thin-walled cantilever probe is:

$$\delta = \frac{D C_D \frac{1}{2} \rho V^2 L^4}{\pi E D^3 t}$$

If the probe geometry is scaled photographically with the research stage, then this expression yields $\delta \propto D$ after elimination, so the non-dimensional deflection is not affected by

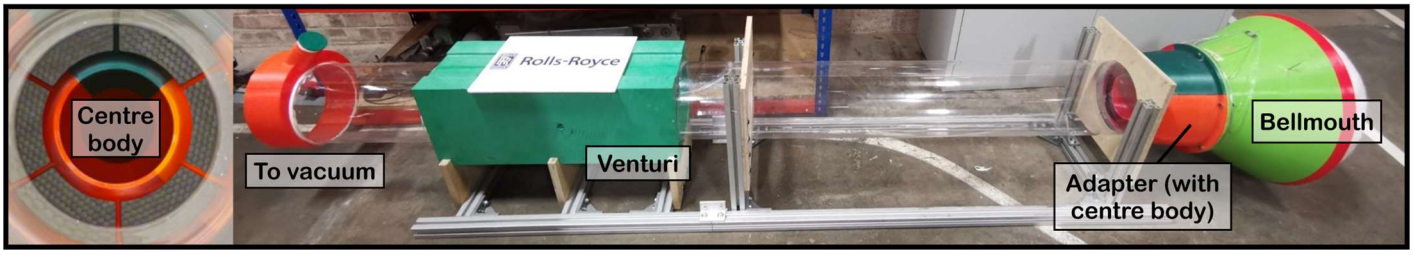

Figure 11: Draw down bellmouth calibration tunnel showing the centre body and struts and venturi location, note that flow is right to left and the flow straightener is obscured by the filtration cloth on the far right

the scaling. The same can be shown for end rotation. The only pitfall is that a smaller probe may be liable to a larger drag coefficient, given the reduced Reynolds number. On the other hand, small diameter hypodermic tubes typically have thicker walls, in compensation.

CONTROL AND OPERATION

A conventional, electric motor driven rig usually employs commercially available control gear for the motor and a simple exit throttle. In this novel turbo-expander rig, a custom control solution is developed to select and maintain shaft speed to map out constant speed characteristic lines.

Two motorised valves are used and are shown in the block diagram of Figure 2. Approximately speaking, the bypass valve controls the non-dimensional speed by adjusting the vacuum level behind the power turbine and therefore its pressure ratio. The bleed valve controls the compressor flow coefficient as the turbine flow rate does not vary as much. However, the relationship is not exact and as the bleed valve is closed the shaft speed increases slightly. To achieve a constant non-dimensional speed measurement of the research compressor this speed is controlled by opening or closing the bypass valve in real time as the variable bleed is adjusted.

The bleed system is shown in detail in Figure 10. Bleed air exits the slot on the casing and is channelled via the annular duct shown in yellow into the plenum shown in green. The vanes in the annular duct are structural and non-turning. Both the duct and the plenum are made from selectively laser-sintered Nylon (SLS). The plenum volume helps to maintain circumferential uniformity of bleed pressure. Air is channelled from the plenum to the tailpipe by six flexible hoses which are omitted from Figure 10 for clarity. Plumbing the bleed into the lowest pressure in the system allows for a high bleed rate range. In the tailpipe, a sleeve valve throttles the six hoses simultaneously and equally. Another sleeve valve, which shown as open to the atmosphere, acts as the bypass valve for open loop running. Both sleeve valves are actuated by precision stepper motor driven mechanisms with encoder feedback control.

A radial basis neural network controller is used. This neural network (NN) architecture is selected for its speed in reverse operation and no tendency to overfit the data to create unphysically jiggly surfaces [8]. The network complexity is kept suitably low such that the speed of reverse calculation is sufficiently fast for real-time operation, less than 0.1s. In training, the NN learns to map non-dimensional valve openings to non-dimensional shaft speed. In use, every time the bleed valve moves, the NN reverse calculates the bypass valve position required for the commanded shaft speed and target bleed valve opening. It then actuates the bypass valve automatically, accounting for any mechanical backlash.

The mapping is unique for the research compressor geometry, so a brief calibration / training run is required for each geometry. This run is performed by hand and can be performed in an arbitrary manner so long as the valve ranges are used in full and in combination, so it gives the opportunity to explore the stability envelope of the research stage rapidly. Once complete, constant speed running is possible. Every time an experiment finishes, the NN adds the actual data to its dataset and re-trains, so the quality of control improves with use. There is no danger of overfitting due to the radial basis architecture.

LOW-SPEED RESULTS

To validate the rig's mechanical and control systems, low-speed tests were performed. This section presents results which demonstrate that the rig is controllable and is inherently safe in the event of research compressor stall or blade off.

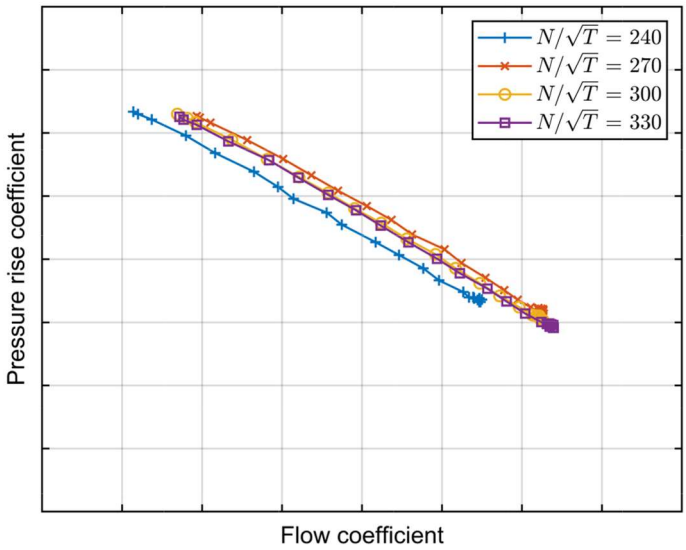

Figure 12: Characteristic lines measured up to 25% speed

Figure 12 and Figure 13 present an experiment where four constant speed characteristics lines, up to 25% design rotational speed, were measured. Figure 12 demonstrates the data quality. The blue curve, being the lowest Reynolds number, is separated from the rest of the curves, possibly due to an early separation on the IGVs. Figure 13 plots the percentage shaft speed error from target, averaged at each data point in Figure 12. Except the

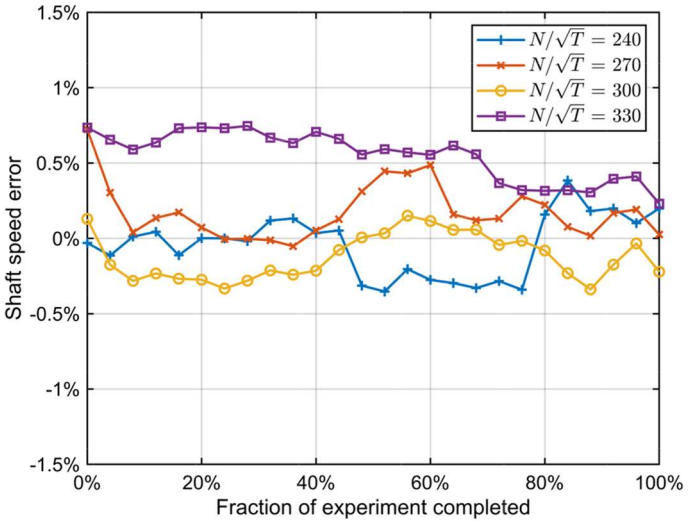

Figure 13: Normalised shaft speed error at each data point throughout the experiment

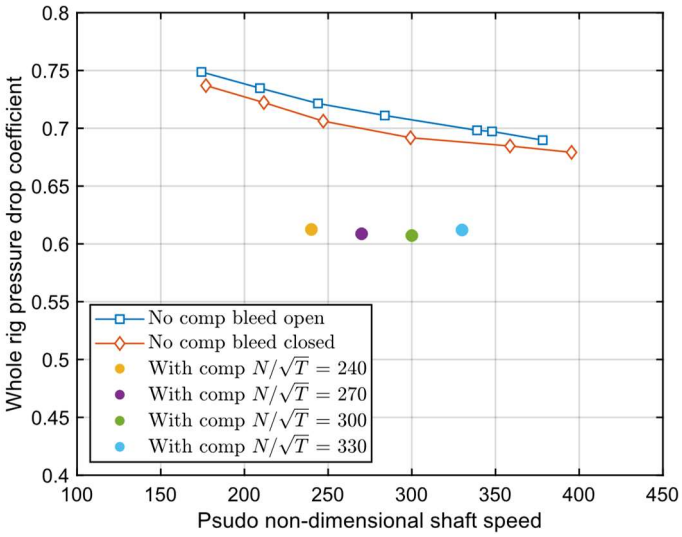

Figure 14: Whole rig pressure drop coefficient with and without compressor rotor

$N/\sqrt{T} = 330$ measurement, the error is within 0.5% throughout and the mean is within 0.3%. The $N/\sqrt{T} = 330$ line has a higher mean error of 0.5% due to a mechanical defect in the bypass valve which has been rectified with a new valve design.

The entire data set behind Figure 12 was acquired in 40 minutes, during which rig was fully stopped three times. The rig, being lightweight and without complexities such as oil-fed ancillaries, can be started and stopped rapidly.

A blade off accident during high-speed testing is extremely hazardous, due to the risk of uncontained fragments and the possibility of a rotating assembly runaway once the load is dropped on the turbine. The small size makes it possible for the casing of this rig to be made relatively thick to contain any possible fragments: see Figure 10. The risk of runaway does not exist as the rig is inherently safe by aerodynamic design.

The rig cannot runaway because it is designed such that the overall pressure drop coefficient is higher than normal without the research compressor rotor so the power turbine is freewheeling. For the same auxiliary compressor working point, this means the rig shaft speed will slow down if the research compressor fails mechanically and the load on the turbine is shed. This is because the velocity triangles are far from design for the downstream blade rows if the research compressor rotor row is not present, causing the downstream rows to stall, resulting in high loss and low mass flow rate. To a lesser extent but with the same argument, the rig will slow down if the research compressor stalls.

To verify the above design intents, experiments are performed without the research compressor rotor attached, simulating a blade off accident. The overall pressure drop coefficient is measured and plotted in Figure 14 as two lines, one with the variable bleed valve fully open and one with the bleed fully closed. Since there is no compression before the bleed slot, having the bleed open or closed makes little difference. This data is compared with the overall pressure drop coefficient with the research compressor rotor attached and the rig running normally, shown in Figure 14 as discrete dots corresponding to the four running speeds presented in Figure 12. The overall pressure drop coefficient without the research compressor rotor is, on average, 16% higher than normal. Extrapolating the lines in Figure 14 to full speed, the maximum possible rotational speed without the research compressor rotor is calculated to be 80% of the design rotational speed, when the auxiliary compressor is run at full speed with no bypass flow. Thus, the risk of an overspeed runaway is physically inexistent.

FUTURE WORK

Experiments are planned to validate mechanical integrity and viability at high speed, to validate and further improve the control system, to demonstrate the ability to repeatably drive into high-speed stall and measure the limit accurately, and to gain experience of rapid testing at high speed.

Should this build prove to be successful at high speed, future work includes building a sister rig which is multi-stage. This will be a reduced-scale test of 3-4 rear high-pressure compressor stages, which is valuable as the HPC rear stages are the first to feel the problems associated with reduction in size as engines move to higher overall pressure ratio and specific work output. However, this presents the challenge that an appropriate Reynolds number may not be attained on this smaller blading if the inlet is at ambient density. Fortunately, at the Whittle Laboratory facilities are in place to allow pressurized closed loop running at a higher density. Infrastructure construction projects are underway for this multistage rig.

CONCLUSIONS

The test case presented in this paper shows that high speed testing can be accomplished at 20% of the power of an engine test if scale is reduced. This power input can be further reduced by using a power turbine to recover the pressure rise from the compressor in a turbo-expander architecture.

The reduced scale reduces both costs and time for manufacture. This means that a rig such as this is ideal for conducting rapid testing: exploring a wider design space or investigating real engine issues in a representative environment.

The rig which has been built is aerodynamically controllable with two variable valves. A bleed upstream of the power turbine allows the research compressor to be driven up its characteristic and into stall. A downstream bypass allows fine control of the shaft rotational speed. This system can be regulated and controlled to the same level of accuracy and steadiness as conventional electric motor driven rigs.

With current standards in manufacture, instrumentation, and controls the authors expect to achieve the same quality of measurements as the low-speed 6ft diameter rigs. Reduced scale testing also allows reproduction of compressibility effects in full and increased flexibility.

ACKNOWLEDGMENTS

The authors acknowledge Rolls-Royce plc for their support and permission to publish this work. Thanks to Nick Atkins, Rob Miller, Colin McFarlane, Chris Hall & Harry Simpson for their direct involvement, discussions and support, additional thanks to colleagues at the Whittle Laboratory for their manufacturing and aerodynamic expertise. This work was supported by the University of Cambridge Harding Distinguished Postgraduate Scholars Programme.

NOMENCLATURE

C_D	Drag coefficient
D	Diameter (m)
	Probe diameter (m)
E	Young's modulus (Pa)
L	Length (m)
M	Mach number
Re	Reynolds number
N	Rotational speed (1/s)
T	Temperature (K)
t	Thickness (m)
V	Velocity (m/s)
$\dot{W}_x$	Shaft power (W)
ρ	Density ($\mathrm{kg/m^3}$)
δ	Deflection (m)

REFERENCES

[1] Robinson, C. J., 1991, "End-Wall Flows and Blading Design for Axial Flow Compressors," PhD Thesis, School of Mechanical Engineering, Cranfield Institude of Technology, Cranfield, UK.

[2] Wisler, D. C., 1985, "Loss Reduction in Axial-Flow Compressors Through Low-Speed Model Testing," Journal of Engineering for Gas Turbines and Power, 107(2), pp. 354–363.

[3] Dickens, T., Taylor, J., Hall, C., and Miller, R., 2021, "Aerodynamic Mitigation of Mechanical Constraints in Small Compressor Blade Profiles," ASME Turbo Expo 2021: Turbomachinery Technical Conference and Exposition, American Society of Mechanical Engineers Digital Collection, doi:10.1115/GT2021-59452.

[4] Goodhand, M. N. and Miller, R. J., 2010, "Compressor Leading Edge Spikes: A New Performance Criterion," Journal of Turbomachinery, 133(021006).

[5] Taylor, J. V., Conduit, B., Dickens, A., Hall, C., Hillel, M., and Miller, R. J., 2019, "Predicting the Operability of Damaged Compressors Using Machine Learning," GT2019, Volume 2A: Turbomachinery, doi:10.1115/GT2019-91339.

[6] Brandvik, T. and Pullan, G., 2010, "An Accelerated 3D Navier–Stokes Solver for Flows in Turbomachines," Journal of Turbomachinery, 133(2).

[7] Spalart, P. and Allmaras, S., 1992, "A One-Equation Turbulence Model for Aerodynamic Flows," 30th Aerospace Sciences Meeting and Exhibit, Aerospace Sciences Meetings, American Institute of Aeronautics and Astronautics.

[8] Clark, C. J., 2019, "A Step Towards an Intelligent Aerodynamic Design Process," Volume 2C: Turbomachinery, American Society of Mechanical Engineers, Phoenix, Arizona, USA, p. V02CT41A033, doi:10.1115/GT2019-91637.